Materials Today: Proceedings 67 (2022) 964–970

Contents lists available at ScienceDirect

Materials Today: Proceedings

journal homepage: www.elsevier.com/locate/matpr

A new method for interpreting Vickers indentation measurements

Asterios K. Kampouris [a], Kimon-Ioannis Lappas [a], Avraam A. Konstantinidis [a,*], Elias C. Aifantis [a,b,c]

[a] Aristotle University of Thessaloniki, Thessaloniki 54124, Greece
[b] Michigan Technological University, Houghton, MI 49931, USA
[c] Mercator Fellow, Friedrich – Alexander University, Erlangen – Nuremberg, Fürth 90762, Germany

ARTICLE INFO

Article history:
Available online 30 June 2022

Keywords:
Vickers indentation
Displacement field, stress/strain fields
Gradient elasticity

ABSTRACT

A new method for interpreting Vickers microindentation data is proposed, based on continuum mechanics and, more precisely, the Gradient Elasticity framework. The main feature is the elastic properties' calculation from the initial (elastic) region of the load vs. depth indentation data, which makes the calculation independent of the maximum indentation depth. This approach deviates significantly from the semi-empirical method of Oliver and Pharr, which calculates the material properties (such as elastic modulus and hardness) from the elastic unloading region, with the calculated values of the elastic modulus and hardness being strongly dependent on the indentation depth and, therefore, giving rise to the so-called indentation size effect (ISE). The proposed framework considers the Vickers indentation as a compression test with a complex geometry, as the pyramidal indenter tip applies load to directions perpendicular to its four faces. An elastic displacement field is initially assumed following Boussinesq's solution before an indent is made, while afterwards the displacement of the material in contact with the tip is assumed to follow the Vickers tip's geometry. The respective von Mises equivalent strain calculated through a continuum mechanics approach can qualitatively capture thin film delamination micrographs and shear band formation, showing the potential of the present formulation to model such microdeformation problems. The traction vector calculated on each of the four sides of the Vickers tip, leads to the generation of load-displacement data, which compare well with experimental indentation data, with the elastic properties (i.e. elastic modulus) thus calculated being in accordance with the corresponding literature values.

Selection and peer-review under responsibility of the scientific committee of the International Conferences & Exhibition on Nanotechnologies, Organic Electronics & Nanomedicine – NANOTEXNOLOGY 2021.

1. Introduction

Various approaches [1–2] use computational routines based on the Oliver-Pharr method or in-situ imaging and SEM/AFM techniques to determine mechanical properties of various materials (steels, metals, elastic solids) via Vickers indentation experiments. The unloading part of the load–displacement (P-h) curves is normally taken into consideration and simplified 1-D models try to theoretically predict the generated P-h experimental data by power law relations using geometric approximations for the pyramidal tips [3].The residual impressions of the Vickers indents normally allow for an estimation of acoustic emission [4] whereas plastic deformation can be described from the volume recovery by thermal annealing, especially in glass bulk samples [5] or during crack propagation [6–8]. During Vickers indentation experiments, the generated residual stresses and fracture toughness of composite coatings have been shown to be affected by a change in the coating thickness [9]. The induced stress fields can be numerically modelled via finite element analysis in conjunction with the Yoffe analytical model [10].

However, in most cases there are deviations from the theoretical predictions of the Oliver-Pharr approach; a detailed analysis of these can be found in [11–15]. A continuum mechanics-based framework capable of modeling indentation imprints, displacement as well as strain/stress fields and associated shear band formation has been recently proposed [16].

The motivation for performing this research is to try to remedy some shortcomings of Vickers indentation. To this end, the gradient elasticity theory (proposed by Aifantis and co-workers

* Corresponding author.
E-mail address: akonsta@civil.auth.gr (A.A. Konstantinidis).

https://doi.org/10.1016/j.matpr.2022.06.242

Selection and peer-review under responsibility of the scientific committee of the International Conferences & Exhibition on Nanotechnologies, Organic Electronics & Nanomedicine – NANOTEXNOLOGY 2021.

[17–19]) was appropriately used as in [20], providing mechanically based strain and stress fields which depend on material parameters, such as the elastic modulus, Poisson's ratio, the maximum elastic deformation as well as the so-called gradient coefficient. Varying these parameters allowed for a means for interpreting thin film delamination and shear band formation near Vickers indentations, as shown recently in [16].

One of the shortcomings that the proposed formulation tried to address is the calculation of the elastic modulus from the elastic loading regime and not from the elastic unloading one. The proposed work avoids making erroneous assumptions on the similarity of axisymmetric tips with the Vickers ones and, on the contrary, it attempts to solve the 3-Dimensional problem of material deformation underneath a Vickers tip by using an upside-down square based pyramid. This leads to the calculation of strain and stress tensors from which an interpretation of the "damage" localization near a Vickers indentation can be made; in addition, through the corresponding traction vector, the value of the elastic modulus can be calculated.

2. Gradient elasticity approach for Vickers indentation

2.1. Deformation field under a Vickers indenter

This work is an extension of the one by Konstantinidis et al [20], in which they started from the deformation field underneath a Berkovich tip, calculated directly from the assumption that as the pyramidal tip penetrates the material, it deforms it in directions perpendicular to the tip's faces, and not in the z direction. Calculating the deformation gradient tensor they were able to calculate the Green strain tensor's components. Next, they assumed classical elasticity as well as gradient elasticity, and they have shown that the σ_{zz} component of the stress tensor in gradient elasticity has the same dependency with the pressure under the tip and, thus, can be used for modeling the tip geometry's effect on indentation data modeling.

Following the same procedure as in [20], the displacement field $\boldsymbol{u^V}(r,\theta,z)$ in cylindrical coordinates under a Vickers tip which has penetrated the material surface by a depth h, is calculated as:

$$\boldsymbol{u^V}(r,\theta,z) = \begin{bmatrix} u_r^V(r,\theta,z) \\ u_\theta^V(r,\theta,z) \\ u_z^V(r,\theta,z) \end{bmatrix} = \begin{bmatrix} \{(h-z)sin68^o - r\,cos68^o\}cos68^o\left[1+\sqrt{sin^2 2\theta}\right] \\ 0 \\ \{(h-z)sin68^o - r\,cos68^o\}sin68^o \end{bmatrix}. \tag{1}$$

A qualitative 3D plot of the displacement field under a Vickers indenter tip is shown in Fig. 1.

Then, calculating the deformation gradient tensor $\boldsymbol{F^V}$ as

$$\boldsymbol{F^V} = \boldsymbol{I} + \nabla \boldsymbol{u^V} = \begin{bmatrix} 1+\partial_r u_r^V & \frac{1}{r}\left(\partial_\theta u_r^V - u_\theta^V\right) & \partial_z u_r^V \\ \partial_r u_\theta^V & 1+\frac{1}{r}\left(\partial_\theta u_\theta^V + u_r^V\right) & \partial_z u_\theta^V \\ \partial_r u_z^V & \frac{1}{r}\partial_\theta u_z^V & 1+\partial_z u_z^V \end{bmatrix}, \tag{2}$$

the infinitesimal strain tensor, $\boldsymbol{\varepsilon^V} = \frac{1}{2}\left[\left(\boldsymbol{F^V}\right)^T + \boldsymbol{F^V}\right] - \boldsymbol{I}$, is derived as

$$\boldsymbol{\varepsilon^V} = \begin{bmatrix} \varepsilon_{11}^V & \varepsilon_{12}^V & \varepsilon_{13}^V \\ \varepsilon_{21}^V & \varepsilon_{22}^V & \varepsilon_{23}^V \\ \varepsilon_{31}^V & \varepsilon_{32}^V & \varepsilon_{33}^V \end{bmatrix}, \tag{3}$$

with

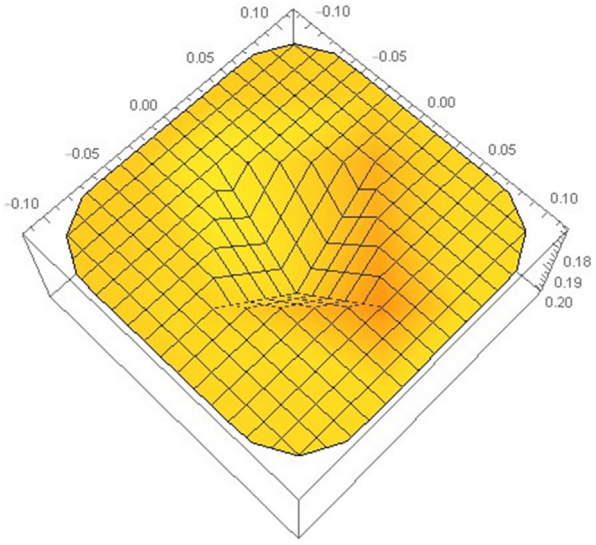

Fig. 1. Qualitative 3D plot of the displacement field under a Vickers indenter tip.

$\varepsilon_{11}^V = -0.14033(1+|sin2\theta|)$; $\varepsilon_{22}^V = (0.34733/r)[(h+z) - 0.404027\,r](1+|sin2\theta|)$;

$\varepsilon_{33}^V = -0.85967$; $\varepsilon_{12}^V = \varepsilon_{21}^V = (0.17366/r|sin2\theta|)\,[(h+z) - 0.404027\,r]\,sin[4arctan(cos\theta/sin\theta)]$;

$\varepsilon_{13}^V = \varepsilon_{31}^V = -0.17366\,(2+|sin2\theta|)$; $\varepsilon_{23}^V = \varepsilon_{32}^V = 0$.

2.2. Introduction of initial elasticity (Boussinessq's solution)

In [16] it was assumed that for very small forces the Vickers tip just "pushes" the material surface elastically up to a maximum displacement h_{el}, without forming an indent. While, when the tip starts forming an indent, the material next to the tip is elastically deformed and this elastic deformation seems to "move" radially away from the tip by the radius a of the imprint. Thus, it is assumed that the elastic displacement of material points around the tip (and not in contact with it) now starts from the Vickers' edges instead of its apex, i.e. is given by the same function but with $r \to r+a$. More precisely, the material points in contact with the Vickers tip exhibit a displacement given by Eq. (1) plus the aforementioned maximum elastic displacement in the z direction, i.e. $u_z^V + h_{el}$, while the displacement of the material points not in contact with the tip is given by Boussinessq's solution [21], but for $r \to r+a$. Then, the total displacement $(u_r^{tot}, u_\theta^{tot}, u_z^{tot})$ is a superposition of the Boussinessq displacement field, for material points not in contact with the tip, and the one dictated by the Vickers geometry $(u_r^V, u_\theta^V, u_z^V)$ given by Eq. (1), for material points in contact with the tip, as:

$$\begin{aligned} u_r^{tot} &= u_r|_{r\to r+a} + u_r^V; \\ u_\theta^{tot} &= u_\theta|_{r\to r+a} + u_\theta^V = 0; \\ u_z^{tot} &= u_z|_{r\to r+a} + u_z^V + h_{el}. \end{aligned} \tag{4}$$

The respective plot of the total displacement under a Vickers tip given by Eq. (4) is shown in Fig. 2.

In this case, the infinitesimal strain tensor under the Vickers tip in cylindrical coordinates is given by

$$\boldsymbol{\varepsilon} = \begin{bmatrix} \varepsilon_{11} & \varepsilon_{12} & \varepsilon_{13} \\ \varepsilon_{21} & \varepsilon_{22} & \varepsilon_{23} \\ \varepsilon_{31} & \varepsilon_{32} & \varepsilon_{33} \end{bmatrix}, \tag{5}$$

with its components being functions of space and material characteristics (Poisson's ratio, maximum elastic displacement before the formation of an indent) given by

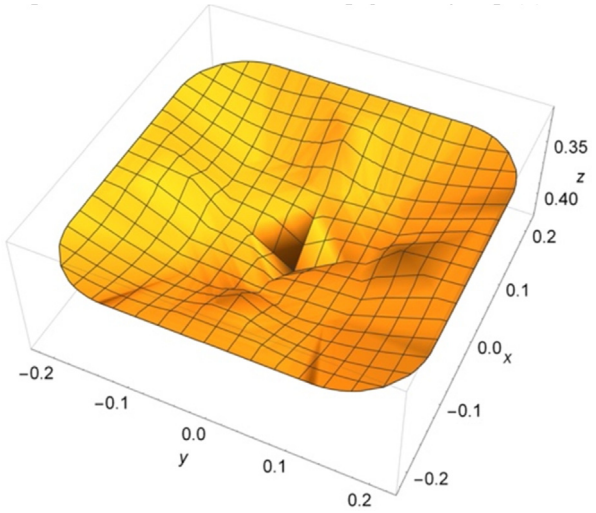

Fig. 2. Qualitative 3D plot of the displacement field under a Vickers indenter tip, including the Boussinessq's [21] solution.

$$\varepsilon_{11} = \frac{h_{el}^2\left[z\left[4r^4(\nu-1)+2r^2z^2(3\nu-1)+z^4(2\nu-1)\right]+\left(r^2+z^2\right)^{5/2}(1-2\nu)\right]}{2r^2\left(r^2+z^2\right)^{5/2}(1-\nu)} - 0.14033$$
$$(1+|sin2\theta|);$$
$$\varepsilon_{22} = \frac{h_{el}^2\left[\left[2\left(zr^2-\left(r^2+z^2\right)^{3/2}\right)(1-\nu)-z^3(2\nu-1)\right]\left(r^2+z^2\right)+\left(r^2+z^2\right)^{5/2}\right]}{2r^2\left(r^2+z^2\right)^{5/2}(1-\nu)} + \frac{0.34733}{r}$$
$$[(h+h_{el}+z)-0.404027\,r](1+|sin2\theta|);$$
$$\varepsilon_{33} = \frac{h_{el}^2\,z\left[2\left(r^2+z^2\right)\nu-3z^2\right]}{2\left(r^2+z^2\right)^{5/2}(1-\nu)} - 0.85967;$$
$$\varepsilon_{12}=\varepsilon_{21} = \frac{0.17366\,[(h+h_{el}+z)-0.404027\,r]\,sin[4arctan(cos\theta/sin\theta)]}{r|sin2\theta|};$$
$$\varepsilon_{13}=\varepsilon_{31} = \frac{-3h_{el}^2rz^2}{2\left(r^2+z^2\right)^{5/2}(1-\nu)} - 0.17366\,(2+|sin2\theta|);\ \varepsilon_{23}=\varepsilon_{32}=0,$$

where (r,θ,z) are cylindrical coordinates (chosen for brevity in the components' expressions), ν denotes Poisson's ratio, h the penetration depth and h_{el} the maximum elastic displacement before an indent is formed, while the Vickers' tip apex angle was taken as $\varphi = 68^0$.

From the infinitesimal strain tensor, a local (microscopic) strain tensor, accounting for heterogeneity effects within the material representative volume element (RVE) may be assumed in the form $\boldsymbol{\varepsilon}^{\boldsymbol{grad}} = \boldsymbol{\varepsilon} - \ell^2\nabla^2\boldsymbol{\varepsilon}$, with ℓ denoting an internal length characterizing the heterogeneity of RVE, along the lines of internal length gradient (ILG) mechanics approach [22]. Then, the equivalent von Mises strain is calculated from the $\boldsymbol{\varepsilon}^{\boldsymbol{grad}}$ strain tensor as [16]

$$\varepsilon_{eq} = \frac{\sqrt{2}\sqrt{\left(\varepsilon_{11}^{grad}-\varepsilon_{22}^{grad}\right)^2+\left(\varepsilon_{22}^{grad}-\varepsilon_{33}^{grad}\right)^2+\left(\varepsilon_{33}^{grad}-\varepsilon_{11}^{grad}\right)^2+6\left(\left(\varepsilon_{12}^{grad}\right)^2+\left(\varepsilon_{23}^{grad}\right)^2+\left(\varepsilon_{13}^{grad}\right)^2\right)}}{3}, \tag{6}$$

which is, again, a function of the cylindrical coordinates (r,θ,z), the Poisson's ratio ν, the maximum elastic displacement before an indent is formed h_{el}, the internal length ℓ as well as of the penetration depth h.

It is noted that although the internal length ℓ is usually characterizing material heterogeneity, in this case it also corresponds to non-local interactions due to the heterogeneous loading applied by the non-flat tip geometry [16].

Next, gradient elasticity [17–19] was assumed for modeling the relation between the strain and stress tensors underneath the Vickers tip, where the so-called gradient coefficient c in this case can be thought of as the square of the respective internal length ℓ, i.e. $c = \ell^2$. The stress tensor calculated using the above infinitesimal strain components reads:

$$\boldsymbol{\sigma}^{grad} = \lambda(tr\boldsymbol{\varepsilon})\mathbf{1} + 2\mu\boldsymbol{\varepsilon} + c\nabla^2[\lambda(tr\boldsymbol{\varepsilon})\mathbf{1} + 2\mu\boldsymbol{\varepsilon}], \tag{7}$$

with its components being parametric functions of space and material characteristics (Poisson's ratio ν, maximum elastic displacement h_{el} before the formation of an indent, Lamé constants λ, μ or, equivalently, elastic modulus E), as well as of the gradient coefficient c. Due to their cumbersome form, the stress components are not given here, but they can be directly calculated by Eqs. (5) and (7). A typical 3D contour plot of the σ_{zz}^{grad} component for specific values of h_{el}, λ and c under a Vickers tip is illustrated in Fig. 3.

2.3. Elastic modulus calculation

A novel aspect of the proposed formulation is the calculation of the elastic modulus from the first part of the loading curve, i.e. within elasticity, in contrast with the common practice of calculating it from the elastic unloading regime [23]. For the elastic modulus to be calculated, the traction vector at the direction perpendicular to one of the tip's faces is first calculated. This is done by taking the inner product of the normal to the face unit vector with the stress tensor:

$$\boldsymbol{T}^{(n_{face})} = n_{face}\cdot\boldsymbol{\sigma}^{grad}, \tag{8}$$

with the normal to one of the Vickers tip's faces unit vector given by $n_{face} = \left[cos68^o \quad \pi/4 \quad sin68^o\right]^T$, in cylindrical coordinates.

The traction vector at the direction perpendicular to the tip's face is considered to be herein the mode of loading in an indentation experiment. More precisely, the deformation field was calculated based on the assumption that as the tip penetrates the material, it deforms the material on directions perpendicular to its faces, and not in the z direction. Thus, a 3-D formulation of the indentation problem is considered, in contrast to the common practice of assuming that the deformation is taking place perpendicular to the specimen's surface, rendering the test to be one-dimensional.

From Eq. (8) the traction vector is calculated through the stress tensor on the same direction that the deformation is assumed to take place, and is a function of space. Its numerical integration over the tip's face provides the mean force over the face area $\left(\bar{\boldsymbol{T}}^{(n_{face})}\right)$, which can be multiplied with the area (A_{face}) to lead to the mean load applied by one of the tip's faces to the material, as:

$$\bar{\boldsymbol{T}}^{(n_{face})}A_{face} = P(h;E,\nu,h_{el},c), \tag{9}$$

which is a parametric function of the indentation depth, with the parameters being, again, the modulus of elasticity (or the related first Lamé constant) the Poisson's ratio, the maximum elastic displacement and the gradient coefficient. This mean force value is actually ¼ of the total force applied by the indenter on

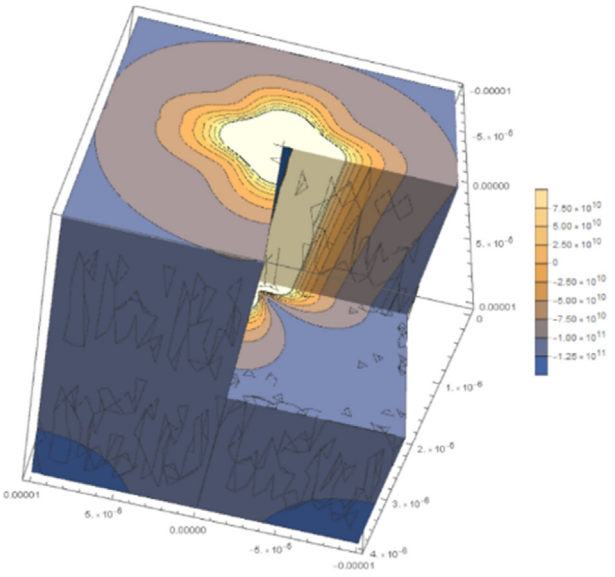

Fig. 3. A 3-D contour plot of the σ_{zz}^{grad} component for specific values of the h_{el}, λ and c under a Vickers tip.

the material's surface. It turns out that the mean force vs. penetration depth relation coming from the proposed formulation has the following form:

$$P(h; E, \nu, h_{el}, c) = 1.65\, f(E, \nu, h_{el}, c)\, (h - h_{el})^2, \tag{10}$$

where $f(E, \nu, h_{el}, c)$ is a function of λ, ν, h_{el}, c, with a cumbersome form and, thus, not explicitly given herein. Equation (10) is a load vs. indentation depth relation which will be compared with experiments.

Comparing the predictions of Eq. (10) on the load vs. depth relation with respective indentation measurements data results to the estimation of the various parameters of the $f(E, \nu, h_{el}, c)$ function. This is actually a novel way for elastic modulus' estimation from the elastic part. A second novelty concerning the theoretical load vs. depth prediction of Eq. (10), is that from the fitted elastic loading curve an estimate of the depth where the elasto-plastic transition takes place could possibly also lead to a depth threshold after which the bulk material hardness should be calculated.

2.4. Sensitivity analysis of equivalent strain

In [16] a 2D parametric study investigated the dependence of the von Mises strain and stress fields on different values of their parameters (E, ν, h_{el}, ℓ). In this section we first test the sensitivity of the equivalent strain given by Eq. (6). It turns out that its dependence on the values of the Poisson's ratio is not significant. Fig. 4 shows the equivalent strain contours on the $x-y$ plane $(z = 0)$, as well as on the $x-z$ plane $(x = 0)$, for different maximum elastic depth–to–indentation depth ratios, namely $h_{el}/h = 0.1$, $h_{el}/h = 0.11$, i.e. a 10% variation of the h_{el} parameter for a given indentation depth h value, as well as with a simultaneous 50% variation of ℓ, namely $\ell = 1nm$, $\ell = 1.5nm$.

It can be seen from Fig. 4 that there is no sensitivity of the model's prediction for the equivalent strain by Eq. (6) on changes of the values of the maximum elastic depth h_{el} as well as of the internal length ℓ.

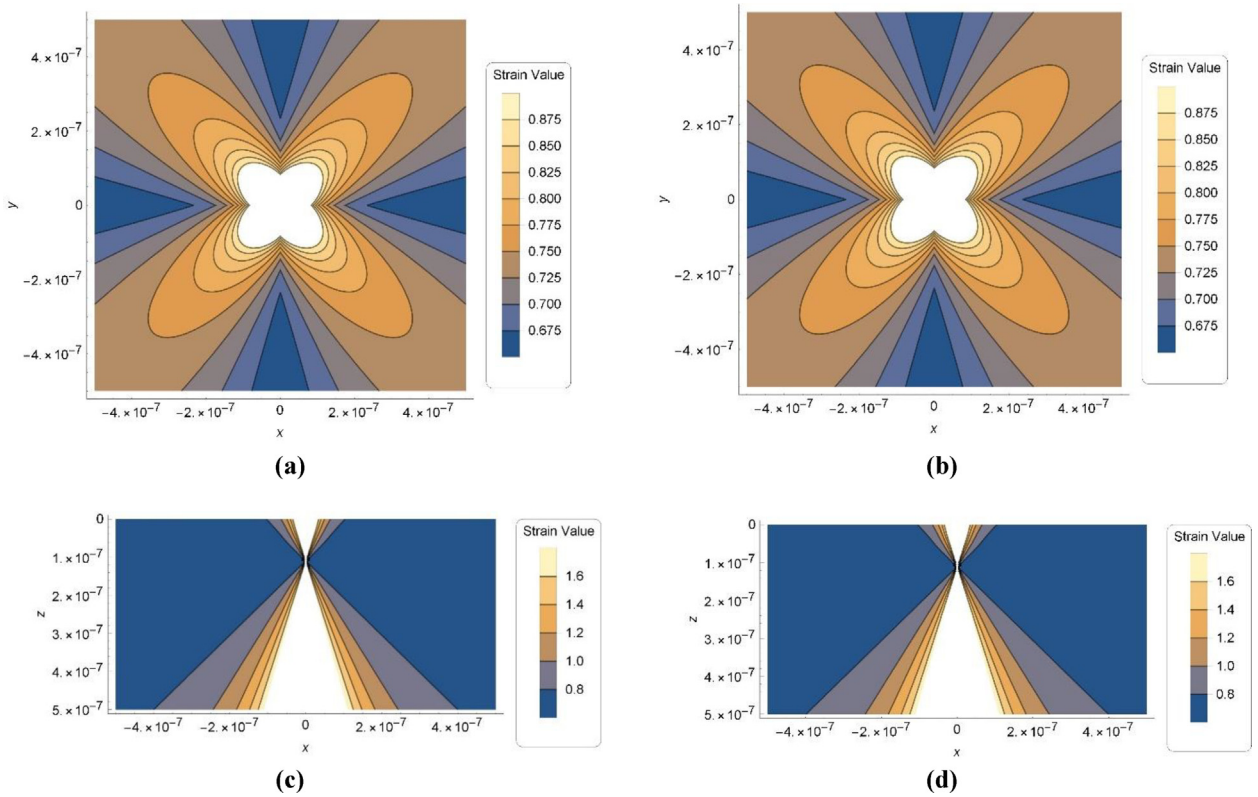

Fig. 4. Contour plots of the equivalent strain predicted by Eq. (6) for: **(a)** the $x-y$ plane for $h = 100nm, h_{el} = 10nm, \ell = 1nm$; **(b)** the $x-y$ plane for $h = 100nm, h_{el} = 11nm, \ell = 1.5nm$; **(c)** the $x-z$ plane for $h = 100nm, h_{el} = 10nm, \ell = 1nm$; **(d)** the $x-z$ plane for $h = 100nm, h_{el} = 11nm, \ell = 1.5nm$. For all plots the Poisson's ratio was taken as $\nu = 0.25$.

The sensitivity of the model's predictions of Eq. (10) on the load vs. depth with small (10%) changes in the values of the various parameters was also checked. It again turns out that the model's predictions do not vary significantly with small variations in the value of the Poisson's ratio, which in all cases is taken equal to $\nu = 0.25$. The following cases are considered: a) $h_{el} = 10nm$, $E = 100GPa$, $c = 100nm^2$, b) $h_{el} = 11nm$, $E = 100GPa$, $c = 100nm^2$, c) $h_{el} = 10nm$, $E = 100GPa$, $c = 110nm^2$, and d) $h_{el} = 10nm$, $E = 110GPa$, $c = 100nm^2$, i.e. changing the values of h_{el}, E, c by 10%. The load vs. displacement plots for the aforementioned cases are shown in Fig. 5, indicating that the model's predictions are not sensitive to small variations of the values of the h_{el}, c parameters, and there is a small sensitivity on the modulus of elasticity value, but only for large indentation depths.

But in order for the potential of Eq. (10) predictions to be shown, load vs. depth predictions with large differences in the aforementioned parameters values are depicted in Fig. 6. It can be seen from Fig. 6 that by changing the parameter values one

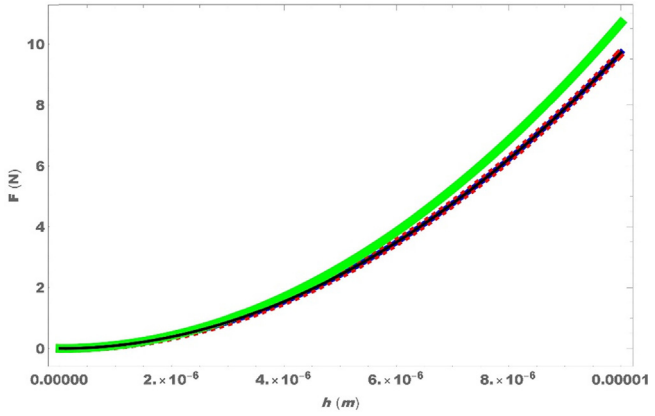

Fig. 5. Sensitivity analysis of the load vs. displacement predictions of Eq. (10) for $h_{el} = 10nm$, $E = 100GPa$, $c = 100nm^2$ (blue line), $h_{el} = 11nm$, $E = 100GPa$, $c = 100nm^2$ (red dashed line), $h_{el} = 10nm$, $E = 100GPa$, $c = 110nm^2$ (black line), and $h_{el} = 10nm$, $E = 110GPa$, $c = 100nm^2$ (green line). There is no sensitivity on small changes of the h_{el}, c parameters, and a small sensitivity on E for large indentation depths. For all cases the Poisson's ratio was taken as $\nu = 0.25$. (For interpretation of the references to colour in this figure legend, the reader is referred to the web version of this article.)

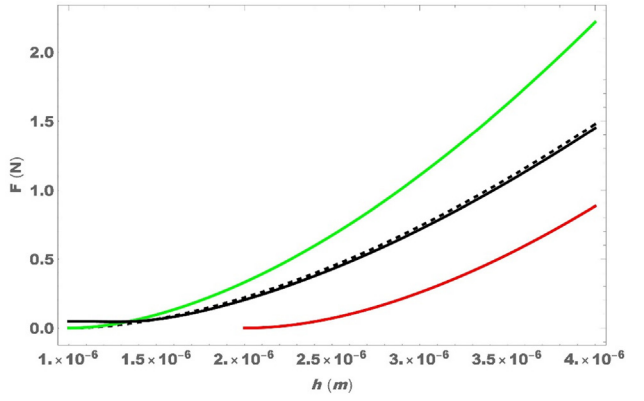

Fig. 6. Prediction of load – depth curves by Eq. (10) for different set of parameters E, h_{el}, c. Black dashed curve for $h_{el} = 1\mu m, E = 100GPa, c = 1nm^2$. Setting $h_{el} = 2\mu m$ (red curve) leads to a "shift" of the prediction towards larger depth values; increasing the elastic modulus to $E = 100GPa$ (green curve) increases the prediction's curvature; setting $c = 55nm^2$ (black solid curve) leads to a small "rotation". (For interpretation of the references to colour in this figure legend, the reader is referred to the web version of this article.)

can approximate experimental load vs. displacement Vickers data, with an ultimate goal of calculating the modulus of elasticity E, as done in the next Section of this work. More precisely, increasing (decreasing) the h_{el} parameter leads to a "shift" of the load vs. depth prediction to larger (smaller) depths, increasing (decreasing) the E parameter leads to predictions with larger (smaller) curvature, while an increase (decrease) of the c values leads to a small "rotation" of the load vs. depth prediction of Eq. (10).

3. Validation of the proposed formulation

3.1. Shear band formation modeling

In [1] aluminum specimens were experimentally investigated with a Vickers indenter. Fig. 7a shows a Vickers' impression on aluminum for a load of 255 mN, with small characteristic shear bands around it, which are semicircular and "embrace" each side from the one edge to the other. The Young's modulus and Poisson's ratio are given equal to 70 GPa and 0.33, respectively [1], while the indentation depth was calculated as the mean diagonal / 7, and found approximately equal to 2850 nm.

The von Mises equivalent strain of Eq. (6) is used to capture the Vickers impression. The theoretical model's prediction can be seen in Fig. 7b, where the maximum elastic deformation was taken equal to $h_{el} = 60nm$ and the gradient coefficient value was taken as $c = 324\mu m^2$.

As can be seen in Fig. 7, there is a striking qualitative as well as quantitative agreement between the theoretical model's predictions of Eq. (6) and the reported in [1] Vickers impression with the surrounding shear bands, indicating the potential of the proposed formulation to describe deformation patterns underneath a Vickers tip.

3.2. Modeling load-displacement curves – calculation of elastic modulus

Based on the theoretical framework presented in the previous section, we compared our model's predictions on load vs. depth as given by Eq. (10), with respective Vickers indentation data on Alumina and Glass samples [3], as shown in Fig. 8.

Since the proposed formulation is based on gradient elasticity, only the initial loading part pertaining to the material's elastic behavior is of interest. Although this "elastic" region for the material in contact with the tip is very difficult to be defined, it is considered to start when the imprint starts to form, i.e. when $h \geq h_{el}$, and ends when all the material underneath the tip has yielded. Thus, only a number of the initial load vs. depth measurements can be approximated through the proposed formulation, providing this way an indirect estimation of the material's elastic region. In the two test cases considered, the theoretical predictions coincided with the experimental measurements for depths up to 9 μm and 4.5 μm for the Alumina and Glass specimens, respectively, indicating an estimate of the "elastic" region of the material under the Vickers tip.

At larger depths all the material under the Vickers tip will have already yielded. This is considered to be a loading threshold for the material's surface similar to the yield stress in the bulk material. Above this load (or the corresponding depth) level the asymptotic (bulk) value of hardness should be reached.

It is noted at this point that the volumetric ratio between a Vickers pyramid tip and an ideal rectangular parallelepiped, is $V_V/V_P \approx 1/6$, which actually means that the corresponding strain induced by Vickers indentation is 6 times smaller than the one induced by compression. This, in turn, means that in order to produce the same level of strain, the depth of a Vickers indentation

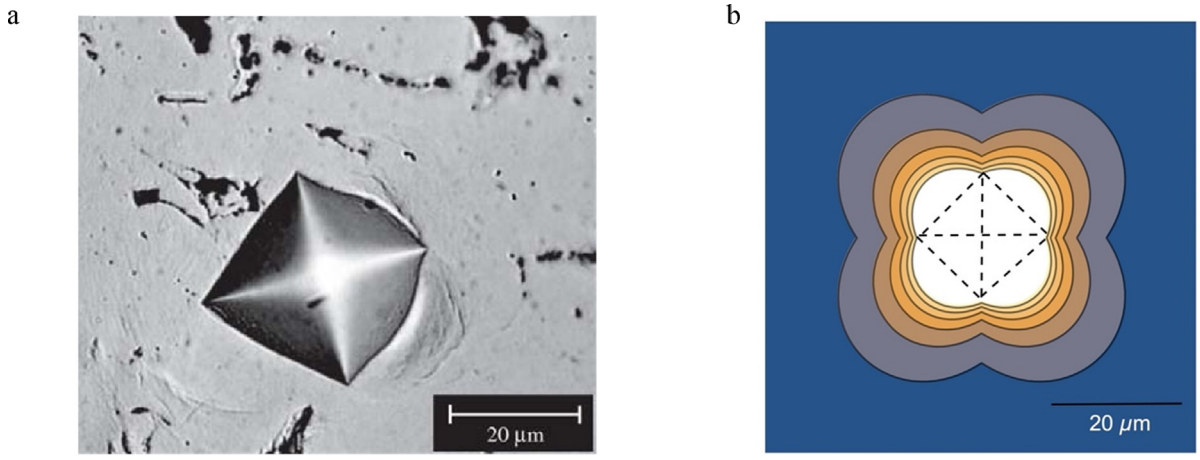

Fig. 7. (a) Vickers impression on an aluminum sample [1]; (b) Theoretical prediction of the equivalent von Mises strain derived from the gradient infinitesimal strain tensor, as predicted by Eq. (6) at z = 0, with $h_{el} = 60nm$ and $c = 324\mu m^2$. A qualitative / quantitative similarity is obvious. The out-of-plane tip shape is shown with dashed lines.

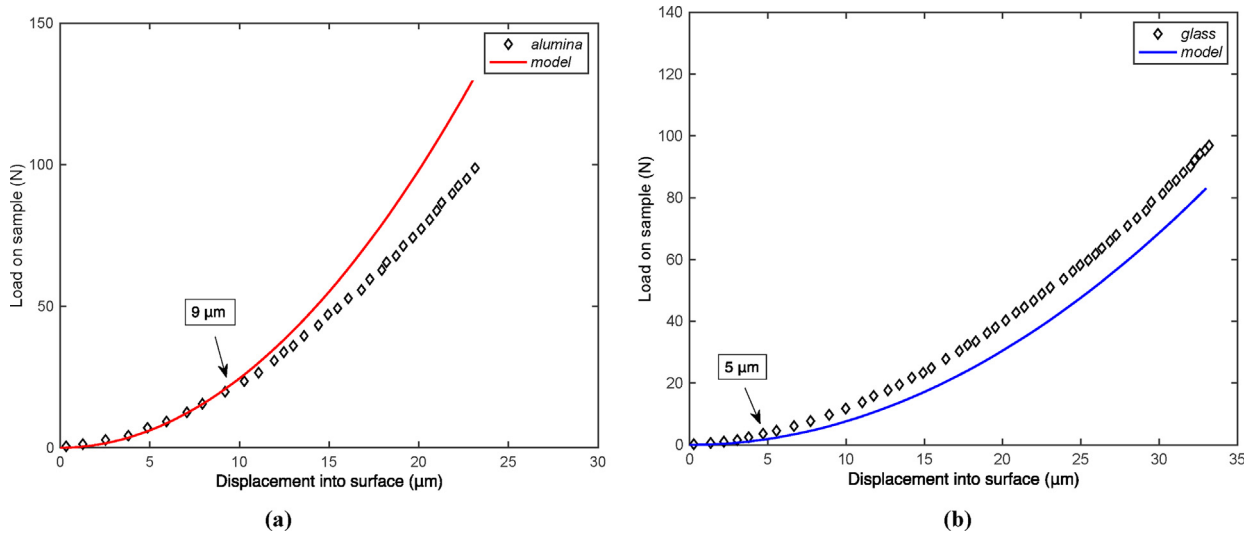

Fig. 8. Fitting the initial (elastic) part of the load – displacement measurements [3] of **(a)** Alumina, and **(b)** Glass samples, for elastic modulus calculation. The predictions of the theoretical model were taken with $h_{el} = 10nm,\ \nu = 0.21,\ c = 1000nm^2,\ E = 215GPa$ for the Alumina sample, as well as $h_{el} = 10nm,\ \nu = 0.23,\ c = 800nm^2,\ E = 75GPa$ for the Glass sample.

should be 6 times larger than the corresponding depth during indentation with a flat tip (similar to compression). Now, the values of 9 μm and 4.5 μm for the Alumina and Glass data, respectively, multiplied by 6 correspond to 54 μm and 27 μm, respectively, above which the asymptotic value of the hardness is actually reached, as also reported in [3]. This is another indication of the potential of the proposed formulation.

The various parameters used in the comparison between the theoretical predictions of Eq. (10) with the experimental data [3], shown in Fig. 8, were: $h_{el} = 10nm,\ \nu = 0.21,\ c = 1000nm^2,\ E = 215GPa$ for the Alumina sample, as well as $h_{el} = 10nm,\ \nu = 0.23,\ c = 800nm^2,\ E = 75GPa$ for the Glass sample. The elastic modulus estimated in each case is in very good agreement with values reported in the literature.

4. Conclusions

In the present work an initial attempt is made to formulate a 3D continuum mechanics-based approach for interpreting load vs. depth data measured during Vickers indentation. In this approach it is assumed that the deformation underneath the tip is taking place in directions perpendicular to the tip's faces and forming self-similar indents. The displacement field of the material points in contact with the Vickers tip is supposed to follow the real (upside-down pyramid with rectangular base) tip's geometry, with no approximations made.

The present work aims at providing a different setting for: a) providing displacement/strain/stress fields near the Vickers tip; b) providing an estimate of the elastic region underneath the tip; c) calculating the modulus of elasticity from elastic loading, and the theoretical predictions seem to provide results in accordance with Vickers indentation experiments.

Of course, the proposed formulation concerns only the calculation of displacement, strain and stress fields, as well as of the elastic modulus based on Vickers indentation data. Erroneous measurements of the load and the depth during Vickers indentation, possibly due to a blunt tip or a rough specimen surface, are not dealt with in the proposed formulation. As all other indentation approaches (e.g. [23]) the proposed formulation assumes, as a first approximation, an ideal tip geometry, as well as a perfectly flat and homogeneous specimen.

But the incorporation of an internal length through gradient elasticity [22] in Eqs. (6) and (10) provides to the proposed formulation a means for taking into account material heterogeneity. As was mentioned earlier, this internal length although originally used to account for material heterogeneity, it could also incorporate the effect of inhomogeneous loading due to a non-flat or non-ideal tip shape. The potential of the proposed formulation to take into account, through the incorporated internal length, material heterogeneity and/or heterogeneous loading conditions (possibly due to tip bluntness or specimen roughness) should be explored and will be the subject of a future publication.

CRediT authorship contribution statement

A.K. Kampouris: Investigation, Visualization, Writing – original draft. **K.-I. Lappas:** Investigation, Visualization. **A.A. Konstantinidis:** Conceptualization, Methodology, Writing – review & editing. **E.C. Aifantis:** Resources, Writing – review & editing.

Declaration of Competing Interest

The authors declare that they have no known competing financial interests or personal relationships that could have appeared to influence the work reported in this paper.

Acknowledgements

This research is co-financed by Greece and the European Union (European Social Fund- ESF) through the Operational Programme ‘‘Human Resources Development, Education and Lifelong Learning 2014-2020” in the context of the project ‘‘Modifying the Conceptual Framework for Nano-Indentation: Application to Thin Films Used in Organic Electronics” (MIS 5047851).

References

[1] A.R. Franco Jr, G. Pintaúde, A. Sinatora, C.E. Pinedo, A.P. Tschiptschin, Mater. Res. 7 (2004) 483–491.
[2] Y.Y. Lim, M.M. Chaudhri - Mechanics of Materials, (2006) – Elsevier.
[3] B. Xu, J. Gong, Key Eng. Mater. 492 (2012) 9–13.
[4] N.H. Faisal, R.L. Reuben, R. Ahmed, Meas. Sci. Technol. 22 (2010) 015703.
[5] H. Sawasato, S. Yoshida, T. Sugawara, Y. Miura, J. Matsuoka, J. Ceram. Soc. Jpn. 116 (2008) 864–868.
[6] J. Chevalier, C. Olagnon, G. Fantozzi, J. Mater. Sci. 31 (1996) 2711–2717.
[7] X. Wang, L.K. Venkataraman, C. Tan, Y. Li, Scr. Mater. 194 (2021) 113647.
[8] C.R. Kurkjian, S.M. Allameh, S. Yoshida, Int. J. Appl. Glass Sci. (2021), https://doi.org/10.1111/ijag.16382.
[9] K. Dong, F. Lu, W. Huang, L. Zhu - Vacuum, 2020 – Elsevier.
[10] B.C. Davis, G.S. Glaesemann, I. Reimanis, J. Am. Ceram. Soc. 103 (2020) 7135–7146.
[11] K.D. Sattler, Ed., Handbook of nanophysics: functional nanomaterials (2010). CRC press.
[12] S. Kossman, T. Coorevits, A. Iost, D. Chicot, J. Mater. Res. 32 (2017) 2230–2240.
[13] B.A. Galanov, S.N. Dub, J. Superhard Mater. 39 (2017) 373–389.
[14] P. Haušild, A. Materna, L. Kocmanová, J. Matějíček, Solid State Phenom. 258 (2017) 131–136.
[15] P.S. Phani, W.C. Oliver, G.M. Pharr, J. Mater. Res. 36 (2021) 2137–2153.
[16] A.K. Kampouris, K.-I. Lappas, A.A. Konstantinidis and E.C. Aifantis, Nanoscience and Technology: An International Journal, (2022) in press, doi:https://doi.org/10.1615/NanoSciTechnolIntJ.2021040335
[17] E.C. Aifantis, E.C. Trans, ASME J. Engng. Mater. Techn. 106 (1984) 326–330.
[18] H. Askes, E.C. Aifantis, Int. J. Solids Struct. 48 (2011) 1962–1990.
[19] E.C. Aifantis, Theor. Appl. Mech. Lett. 4 (2014), 051005/1-7.
[20] A.A. Konstantinidis, G. Frantziskonis, H. Askes, E.C. Aifantis, J. Mech. Behav. Mater. 25 (1–2) (2016) 57–60.
[21] M.J. Boussinesq, Application des potentiels a l’étude de l’équilibre et du mouvement des solides élastiques, avec des notes étendues sur divers points de physique mathématique et d’analyse, Gauthier-Villars, Paris, 1885.
[22] E.C. Aifantis, Springer Tracts Mech. Enging. (2021) 417–452.
[23] W.C. Oliver, G.M. Pharr, G.m.,, J. Mater. Res. 7 (1992) 1564–1583.